

Electrically probing photonic bandgap phenomena in contacted defect nanocavities

F. Hofbauer,* S. Grimminger, J. Angele, G. Böhm, R. Meyer, M.C. Amann, and J. J. Finley

*Walter Schottky Institut and Physik Department, Technische Universität München,
Am Coulombwall 3, D-85748 Garching, Germany*

(Dated: November 19, 2018)

Abstract

We demonstrate an electrically tunable two dimensional photonic crystal nanocavity containing InAs self assembled quantum dots. Photoluminescence and electroluminescence measurements are combined to probe the cavity mode structure and demonstrate a local electrical contact to the quantum dots. Measurements performed as a function of the electric field enable us to probe the capture, relaxation and recombination dynamics of photogenerated carriers inside the quantum dots emitting into a modified photonic environment. Furthermore, the two dimensional photonic crystal is probed by spatially dependent photocurrent spectroscopy indicating a $3.5\times$ enhancement of the local radiative lifetime of the QDs inside the photonic crystal environment.

*Electronic address: hofbauer@wsi.tum.de

Nanoengineered photonic materials currently attract widespread interest due to their ability to modify and control spontaneous emission and spatially redirect light from solids.[1] Electrically contacted systems are required for applications in optoelectronics, such as high efficiency LEDs[2] and low threshold nanolasers.[3, 4, 5] However, the need for an electrical contact is less apparent for solid state quantum optics experiments involving quantum dot (QD) emitters[6, 7, 8, 9], where control of the spectral detuning between the QD emitter and the cavity mode ($\Delta\omega = \omega_{QD} - \omega_{cav}$) is needed. To date, a number of ingenious methods have already been developed to coarse tune ω_{cav} in two dimensional photonic crystal (PhC) defect nanocavities.[10, 11] Subsequently, $\Delta\omega$ can be *fine tuned* by varying the temperature to shift ω_{QD} into resonance with ω_{cav} . One drawback of temperature tuning is that large shifts are needed ($\Delta T \sim 30 - 50$ K) to tune $\hbar\Delta\omega$ by a few meV.[7, 8, 9] Since the exciton decoherence rate increases rapidly with temperature[12] methods are required to fine tune $\Delta\omega$ whilst preserving coherence. Electrically contacted cavity-QD systems would enable reversible fine tuning of ω_{QD} using the quantum confined Stark effect[13] and provide a route toward more sophisticated experiments.

In this letter we demonstrate the fabrication and optical investigation of electrically contacted PhC defect nanocavities containing an ensemble of InAs self-assembled QDs. We show that electrical contacts can be established by introducing doped contacts into the waveguide core to form *p-i-n* nanocavity photodiodes. Emission and absorption spectroscopy allow us to probe the competition between carrier capture, relaxation, spontaneous emission and tunneling escape dynamics in a tailored photonic environment.

The samples studied were (Al)GaAs *p-i-n* photodiode structures and nominally consisted of the following layers: Firstly, we deposited a 750 nm thick, n-type ($n = 2 \times 10^{18} \text{cm}^{-3}$, Si-dopant) $\text{Al}_{0.8}\text{Ga}_{0.2}\text{As}$ sacrificial layer followed by a 30 nm thick, n-type GaAs lower contact layer ($n = 2 \times 10^{18} \text{cm}^{-3}$). This was followed by the 110 nm thick intrinsic GaAs waveguide core into the center of which we grew a single layer of QDs by depositing 2.7 ML of InAs at 540°C and a rate of 0.03 ML/s. A 30 nm thick p-type ($p = 2 \times 10^{18} \text{cm}^{-3}$, Be-dopant) GaAs top contact was then grown to complete the structure. After growth we established an Ohmic back contact to the buried n^+ layers and defined $250 \times 400 \mu\text{m}$ photodiode mesas using photolithography and wet etching techniques. $200 \times 200 \mu\text{m}$ windows were opened in the top metallic Ohmic contact for optical access. Inside each window we then formed an array of 25 PhC nanocavities by combining electron beam lithography and $\text{Cl}_2 - \text{Ar}$ reactive

ion etching to define a lattice of cylindrical air holes (radius r) arranged in a hexagonal lattice with period $a = 280$ nm and $r/a = 0.3$. [16] Nanocavities were formed by single missing hole defects with reduced symmetry according to ref. [17]. Finally, suspended PhC membrane structures were fabricated by selectively removing the $\text{Al}_{0.8}\text{Ga}_{0.2}\text{As}$ layer beneath the GaAs waveguide core to leave a free standing, *p-i-n* doped GaAs membrane.

Figure 1(a) insert shows a schematic representation and optical microscope image of the nanocavity photodiode structures. Such devices enable tuning of the static electric field applied along the QD growth direction by tuning the applied bias (V_A) across the *p-i-n* junction. A typical $I - V$ characteristic is presented in figure 1(a), revealing clear diode like behavior as expected with low leakage currents (< 100 pA) in the reverse bias direction and an onset of current flow close to $V_B \sim 1.1 \pm 0.2$ V in the forward bias direction. The relationship between V_A and the static electric field can be approximated by $F = (V_B - V_A)/w$, where w is the width of the intrinsic region.

All optical experiments were performed at 10 K in a confocal microscopy setup that provides $\sim 1\mu\text{m}$ spatial resolution. Figure 1(b) compares the inhomogeneously broadened QD photoluminescence (*PL*) spectra recorded for detection positions both *on* the nanocavity and *off* the PhC on the unpatterned membrane. Both measurements were obtained with **non-resonant** optical excitation (633 nm, ~ 200 W/cm⁻²). In both measurements emission from *s*-, *p*- and *d*- shells of the QDs are observed at ~ 1120 nm, ~ 1060 nm and ~ 1010 nm, respectively. When detected on the nanocavity the dipole like cavity modes are observed.[17] In order to check that a local electrical contact is established to the nanocavity we turned off the laser, forward biased the *p-i-n* diode and recorded electroluminescence (*EL*) spectra with a drive current of $I_{EL} = 35$ mA (see fig 1(b)). The *EL* spectrum exhibits the same characteristic cavity modes which are absent from the measurement recorded away from the cavity. These observations confirm that charge carriers can be injected into the nanocavity through the perforated PhC membrane and that an electrical contact is established to the dots within the structure.

We then *reverse* biased the sample and performed complementary *PL* and photocurrent (*PC*) measurements as a function of the electric field in the range 0 V/cm to 100 kV/cm. Three distinct excitation regimes were explored; **non-resonant** excitation at 633 nm above the bandgap of the PhC matrix material, **quasi-resonant** at 971 nm into the excited states of the QDs and continuum states[14] and **resonant** into the p-shell of the QDs

at 1060 nm. Figure 2(a) shows typical field dependent PL spectra recorded from one of the cavity modes under **non-resonant** excitation. Clearly, the PL is strongest close to the flat band condition ($F = 0$ kV/cm, $V_A = 1.1$ V) and decreases rapidly with increasing field. The quantitative dependence of the integrated PL intensity is plotted in figure 2(b), revealing this rapid quenching behavior. Our findings for non-resonant excitation are compared with similar measurements recorded with **quasi-resonant** excitation. Both curves exhibit the same qualitative behavior, but higher electric fields are required to suppress the PL for quasi-resonant excitation. We quantified these observations by measuring the electric field where the PL reaches half its initial intensity denoted by $F_{1/2}$. We measure $F_{1/2}^{non-resonant} = 16.9 \pm 0.2$ kV/cm and $F_{1/2}^{quasi-resonant} = 49.1 \pm 0.2$ kV/cm, respectively. The observed value of $F_{1/2}^{non-resonant} < F_{1/2}^{quasi-resonant}$ since the intensity of the PL reflects a competition between the various timescales for carrier capture, relaxation and recombination, and that for tunneling escape. Clearly, the observed shift of $F_{1/2}$ to higher field for **quasi-resonant** excitation, when compared with **resonant** excitation, arises since carrier capture is suppressed by the internal electric field. For **resonant** excitation, the PL pathway does not include capture (see figure 2(c)) the PL intensity more closely reflects a trade off between carrier spontaneous recombination and tunneling escape.[15]

In order to cleanly probe the competition between spontaneous emission and carrier tunneling escape we performed PC measurements to complement the PL investigations. The field dependent PC measured with **non-resonant**, **quasi-resonant** and **resonant** excitation is plotted as a function of electric field in 2(b). For each of these excitation regimes the PC increases with F as the system is driven from the situation where carriers are inefficiently extracted into the contacts ($F = 0$ kV/cm) to that where *all* the photogenerated carriers tunnel out of the dots and the PC saturates ($F \sim 60 - 150$ kV/cm). Maintaining the notation $F_{1/2}^{PC}$ to represent the field where the PC reaches 50% of its saturation value, $F_{1/2}^{PC}$ shifts to higher electric field as the excitation becomes more resonant, with values of 16 ± 0.5 kV/cm, 66 ± 0.5 kV/cm and 91 ± 0.5 kV/cm having been measured for the three excitation regimes, respectively. The increase of $F_{1/2}^{PC}$ for tunneling out of the QDs arises since carriers excited more deeply within the dots tunnel less efficiently. For **non-resonant** excitation the normalized PL and PC curves intersect at a value of ~ 0.5 , indicating that all charge carriers which do not become captured into the dots and recombine optically are extracted into the contacts. In contrast, for quasi-resonant excitation the PL and PC

intensity traces intersect at ~ 0.35 indicating the presence of a more complicated relaxation pathway via multiple levels.

For resonant excitation the effective tunneling time primarily competes with radiative recombination, as discussed above, and the value of $F_{1/2}^{PC}$ provides an *electrical measure* for the radiative lifetime of the QDs. In figure 2(d) we compare *PC* measurements recorded on the unpatterned membrane with similar curves recorded from the PhC. The qualitative field dependence of both measurements are identical but $F_{1/2}^{PC}$ clearly shifts to lower fields by $\Delta F = 4.0 \pm 0.5$ kV/cm and 10.1 ± 0.5 kV/cm for **quasi resonant** and **resonant** excitation, respectively. The observation of a shift of $F_{1/2}^{PC}$ to lower field indicates that the spontaneous emission time becomes longer on the photonic crystal compared with the unpatterned membrane. We identify this shift as arising from an enhanced radiative lifetime of QDs emitting inside the 2D photonic bandgap.[1] For **quasi-resonant** excitation the tunneling competes with carrier relaxation process as discussed above, and $F_{1/2}^{PC}$ shifts only by ~ 4 kV/cm. In complete contrast, for non-resonant excitation no shift of $F_{1/2}^{PC}$ is observed since tunneling escape competes with carrier capture, a process that does not depend on the local density of photonic states and is, therefore, the same, irrespective of the local photonic environment. To support these conclusions we modeled the observed *PC* behavior using an adiabatic approximation with decoupled z (parallel to the field) and x, y (in the growth plane) motion. With this approximation, the tunneling probability depends only on the z component of the wave function, and can be modeled using the one-dimensional (1D) WKB approximation. For a 1D confining potential of width L in a perpendicular field F , the tunneling rate R_T is given by

$$R_T = \frac{\hbar\pi}{2m^*L^2} \exp \left[\frac{-4}{3\hbar eF} \sqrt{(2m^*E_I^3)} \right], \quad (1)$$

where E_I is the ionization energy of the electron eigenstate.[13] The normalized *PC* signal (I_{PC}) can then be written as

$$\frac{I_{PC}}{I_{sat}} = \frac{\tau_{rec}}{\tau_{rec} + \tau_{esc}} = \frac{\tau_{rec}R_T}{1 + \tau_{rec}R_T} \quad (2)$$

to reflect the competition between radiative recombination and the local spontaneous emission lifetime (τ_{rec}). We fitted this relation to the *PC* curves recorded from the unpatterned membrane using a measured intrinsic spontaneous recombination time of $\tau_{rec} = 1$ ns[1]

and adjusted the dot height, ionization energy and effective mass to obtain a best fit ($L = 35 \pm 5 \text{ \AA}$, $E_I = 190 \pm 30 \text{ meV}$ and $m^* = 0.049 \pm 0.005m^0$). The same parameters were then used to fit the data recorded from the PhC, changing only the parameter τ_{rec} to obtain the two fits presented on figure 2(d). Using this method, we obtain $\tau_{on}/\tau_{off} = 3.5 \pm 0.3$ demonstrating that the photonic bandgap significantly suppresses spontaneous emission, in good agreement with recent time resolved spectroscopy measurements on similar structures.[1] To further confirm that the observed phenomena arises from the 2D photonic bandgap, we spatially mapped across the the PC region and recorded the field dependent PC curves when subject to resonant excitation. The results of these measurements are presented in fig. 3(a). as a the false color image of $I_{PC}(F)$ data versus detection position. Outside the PhC the $I_{PC}(F)$ curves are independent of detection position since the radiative lifetime is $\sim 1 \text{ ns}$. In contrast, when exciting on the PhC the $I_{PC}(F)$ traces systematically shift to lower field, the strongest shift being observed for $F \sim 10 \text{ kV/cm}$ in the center of the structure. Fitting the data with the WKB method discussed above allows us to extract the local spontaneous emission lifetime. The results of this analysis are presented in figure 3(c), revealing a systematic lengthening of the spontaneous emission lifetime when detecting upon the photonic crystal.

In summary, we have realized electrically contacted two-dimensional PhC defect nanocavities containing an ensemble of InAs self-assembled QDs and studied their fundamental optical properties. The 2D photonic bandgap is probed using a fully electrical approach and comparison of our results with calculations indicate that the spontaneous emission lifetime is suppressed by a factor $\sim 3.5\times$ by the 2D photonic bandgap.

We acknowledge financial support of the Deutsche Forschungsgemeinschaft via the Sonderforschungsbereich 631, Teilprojekt B3 and the German Excellence Initiative via the Nanosystems Initiative Munich (NIM).

-
- [1] M. Kaniber, A. Kress, A. Laucht, M. Bichler, R. Meyer, M.-C. Amann, and J. J. Finley. Appl. Phys. Lett. **91**, 061106 (2007)
- [2] T. N. Oder, K. H. Kim, J. Y. Lin, and H. X. Jiang, Appl. Phys. Lett. **84** 466 (2004).
- [3] B. Ellis, I. Fushman, D. Englund, B. Zhang, Y. Yamamoto, and J. Vučković, Appl. Phys.

- Lett. **90**, 15 (2007)
- [4] H. Hofmann, H. Scherer, S. Deubert, M. Kamp, and A. Forchel, Appl. Phys. Lett. **90**, 2 (2007)
 - [5] S. Strauf, K. Hennessy, M.T. Rakher, Y.S. Choi, A. Badolato, L.C. Andreani, E.L. Hu, P.M. Petroff and D. Bouwmeester. Phys. Rev. Lett. **96**, 127404 (2006)
 - [6] W. Chang, W. Chen, H. Chang, T. Hsieh, J. Chyi, and T. Hsu. Phys. Rev. Lett. **96**, 117401 (2006)
 - [7] T. Yoshie, A. Scherer, J. Hendrickson, G. Khitrova, H. M. Gibbs, G. Rupper, C. Ell, O. B. Shchekin, and D. G. Deppe, Nature **432**, 200 (2004)
 - [8] J. P. Reithmaier, G. Sek, A. Löffler, C. Hofmann, S. Kuhn, S. Reitzenstein, L. V. Keldysh, V. D. Kulakovskii, T. L. Reinecke, and A. Forchel, Nature **432**, 197 (2004)
 - [9] K. Hennessy, A. Badolato, M. Winger, D. Gerace, M. Atatüre, S. Gulde, S. Fält, E. L. Hu, and A. Imamoglu, Nature **445**, 896 (2007)
 - [10] K. Hennessy, A. Badolato, A. Tamboli, P. M. Petroff, and E. Hua, M. Atatüre, J. Dreiser, and A. Imamoglu, Appl. Phys. Lett. **87**, 021108 (2005).
 - [11] S. Strauf, M. T. Rakher, I. Carmeli, K. Hennessy, C. Meier, A. Badolato, M. J. A. DeDood, P. M. Petroff, E. L. Hu, E. G. Gwinn, and D. Bouwmeester, Appl. Phys. Lett. **88**, 043116 (2006).
 - [12] P. Borri, W. Langbein, U. Woggon, V. Stavarache, D. Reuter, and A. D. Wieck. Phys. Rev. **B71**, 115328 (2005)
 - [13] P. W. Fry, I. E. Itskevich, S. R. Parnell, J. J. Finley, L. R. Wilson et al. Phys. Rev. **B62**, 16784 (2001)
 - [14] A. Vasinelli, R. Ferreira, G. Bastard et al. Phys. Rev. Lett **89**, 216804 (2001)
 - [15] P. W. Fry, J. J. Finley, L. R. Wilson, A. Lemaitre, D. J. Mowbray, M. S. Skolnick, M. Hopkinson, G. Hill, and J. C. Clark, Appl. Phys. Lett. **77**, 4344 (2000).
 - [16] A. Kress, F. Hofbauer, N. Reinelt, M. Kaniber, M. Bichler, D. Schuh, G. Böhm, and J. J. Finley, SPIE Proc. **5733**, 114 (2005)
 - [17] Jelena Vučković and Yoshihisa Yamamoto, Appl. Phys. Lett. **89**, 2374 (2003)

Figures

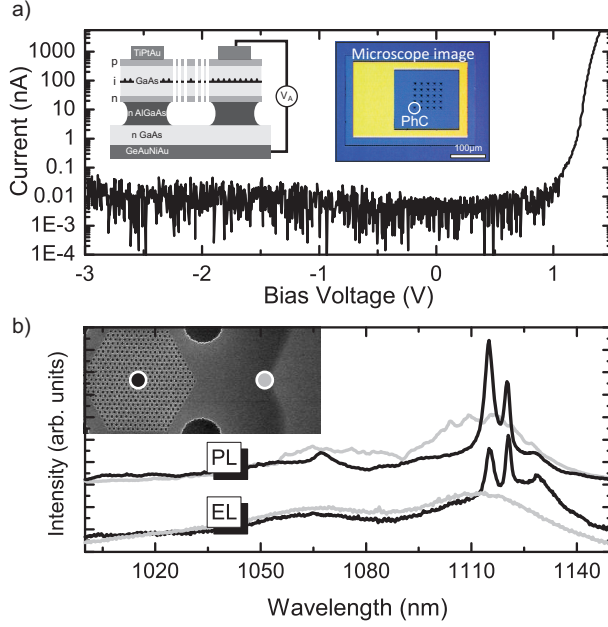


FIG. 1: (a) Typical I - V characteristics recorded from the p - i - n nanocavity photodiodes, (inset) Schematic device structure and microscope image of processed samples. (b) Comparison of μ PL and μ EL measurements obtained *on* the nanocavity and *off* the PhC on the unpatterned membrane

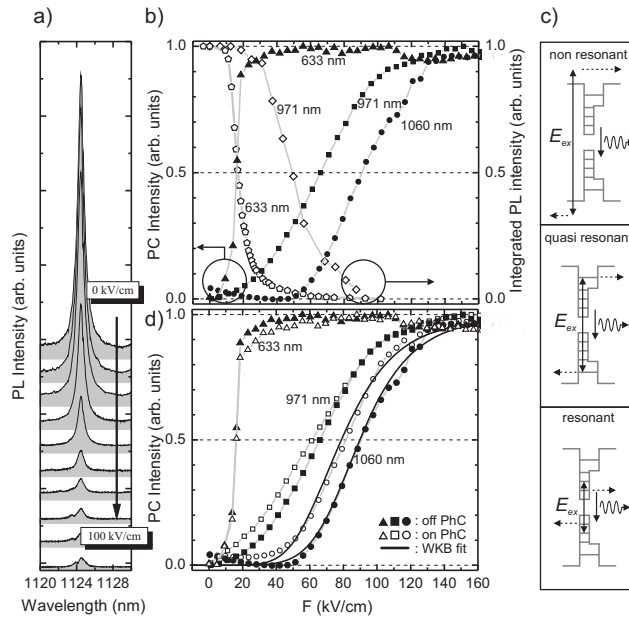


FIG. 2: (a) PL measurements recorded from a cavity mode as a function of the electric field; (b) Electric field dependencies of the PC and PL intensities for non-resonant (633 nm), quasi-resonant (971 nm) and resonant (1060 nm) excitation. (c) Schematic representations of the excitation schemes for non-resonant, quasi-resonant and p-shell excitation (d) Comparison of PC measurements recorded on the PhC and unpatterned membrane revealing the shift of $F_{1/2}$ due to cavity QED effects.

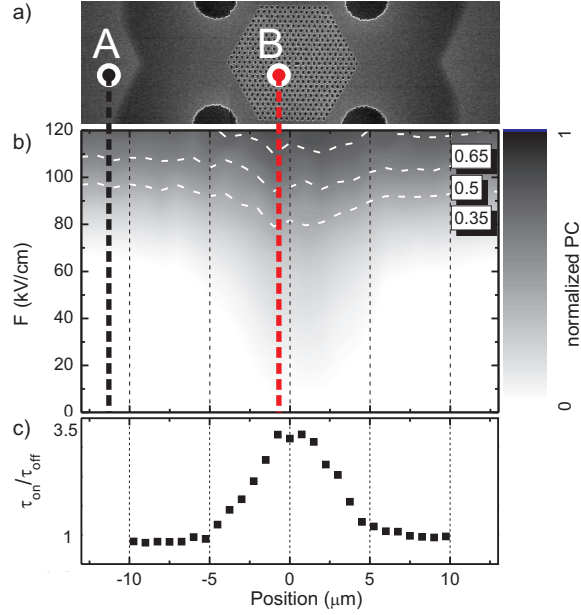


FIG. 3: (a) (b) Spatial mapping of the PC for different electric fields. The points labeled **A** and **B** correspond to the detection positions presented in figure 2(d), on and off the PhC. (c) Local radiative lifetime extracted from the WKB analysis discussed in the text.